

Nanoscale

Accepted Manuscript



This is an *Accepted Manuscript*, which has been through the Royal Society of Chemistry peer review process and has been accepted for publication.

Accepted Manuscripts are published online shortly after acceptance, before technical editing, formatting and proof reading. Using this free service, authors can make their results available to the community, in citable form, before we publish the edited article. We will replace this *Accepted Manuscript* with the edited and formatted *Advance Article* as soon as it is available.

You can find more information about *Accepted Manuscripts* in the [Information for Authors](#).

Please note that technical editing may introduce minor changes to the text and/or graphics, which may alter content. The journal's standard [Terms & Conditions](#) and the [Ethical guidelines](#) still apply. In no event shall the Royal Society of Chemistry be held responsible for any errors or omissions in this *Accepted Manuscript* or any consequences arising from the use of any information it contains.

ARTICLE

Controlled Intracellular Generation of Reactive Oxygen Species in Human Mesenchymal Stem Cells Using Porphyrin Conjugated Nanoparticles

Cite this: DOI: 10.1039/x0xx00000x

Received 00th January 2012,
Accepted 00th January 2012

DOI: 10.1039/x0xx00000x

www.rsc.org/

Andrea S. Lavado,^a Veeren M. Chauhan,^a Amer Alhaj Zen,^b Francesca Giuntini,^c D. Rhodri E. Jones,^d Ross W. Boyle,^e Andrew Beeby,^f Weng C. Chan^{b*} and Jonathan W. Aylott^{a*}

Nanoparticles capable of generating controlled amounts of intracellular reactive oxygen species (ROS), that advance the study of oxidative stress and cellular communication, were synthesized by functionalizing polyacrylamide nanoparticles with zinc (II) porphyrin photosensitisers. Controlled ROS production was demonstrated in human mesenchymal stem cells (hMSCs) through (1) production of nanoparticles functionalized with varying percentages of Zn (II) porphyrin and (2) modulating the number of doses of excitation light to internalized nanoparticles. hMSCs challenged with nanoparticles functionalized with increasing percentages of Zn (II) porphyrin and high numbers of irradiations of excitation light were found to generate greater amounts of ROS. A novel dye, which is transformed into fluorescent 7-hydroxy-4-trifluoromethyl-coumarin in the presence of hydrogen peroxide, provided an indirect indicator for cumulative ROS production. The mitochondrial membrane potential was monitored to investigate the destructive effect of increased intracellular ROS production. Flow cytometric analysis of nanoparticle treated hMSCs suggested irradiation with excitation light signalled controlled apoptotic cell death, rather than uncontrolled necrotic cell death. Increased intracellular ROS production did not induce phenotypic changes in hMSC subcultures.

1. Introduction

Reactive oxygen species (ROS) form through conversion of molecular oxygen, by either (Type I) electron transfer, to produce superoxide, hydrogen peroxide (H₂O₂) and hydroxyl radicals or, (Type II) energy transfer, to produce singlet oxygen.¹ At a cellular level ROS production is highly regulated, typically through confinement of their production to specific organelles, such as the mitochondria,² and management of overproduction with antioxidants.³ Controlled ROS production is known to regulate processes, such as programmed cell death,⁴ initiation of host defences to pathogens⁵ and production of energy *via* the mitochondrial electron transport chain.⁶ Uncontrolled ROS production can propagate chain reactions that can cause irreversible damage to intracellular nucleic acids,⁷ proteins⁸ and lipids⁹ that can result in cellular necrosis,¹⁰ neoplastic mutations¹¹ and neurodegenerative disorders.¹²

The effects of ROS on intracellular processes have been investigated through exogenous addition of H₂O₂.^{13, 14} However, diffusion of H₂O₂ through cell membranes is thought to be restricted,¹⁵ due to tightly regulated membrane channels, such that the effect of exogenous ROS on intracellular effects can be misinterpreted.¹⁶ Therefore, artificially stimulating intracellular ROS, independent of innate and exogenous ROS,

in a controlled manner would enhance the understanding of how oxidative stress contributes to healthy or diseased states. Research into the development of tools to generate ROS in a controlled manner has gathered momentum, such that a number of different strategies have been reported.¹⁷⁻²¹

Polyacrylamide nanoparticles are at the forefront of investigating cellular microenvironments of interest.²² Due to their (1) small size, (2) optical transparency, (3) large surface to volume ratio, and (4) highly versatile matrix, which can be readily engineered to control physicochemical parameters, they can be delivered to biological systems with minimal perturbation.²³ We and others have shown previously how polyacrylamide nanoparticles can be utilized as an analytical tool²⁴⁻²⁷ to target subcellular spaces²⁸⁻³⁰ and provide a real-time measurements of the role of key biological parameters *in situ*.³¹ Polyacrylamide nanoparticles have also been used in photodynamic therapy,^{32, 33} an established therapeutic strategy that is dependent on photo-excitable compounds (photosensitisers) to promote ROS-mediated cell inactivation and tissue damage following irradiation with visible light.³⁴

This article describes the synthesis and characterization of polyacrylamide nanoparticles conjugated to zinc (II) or copper (II) complexed porphyrins that are capable of generating

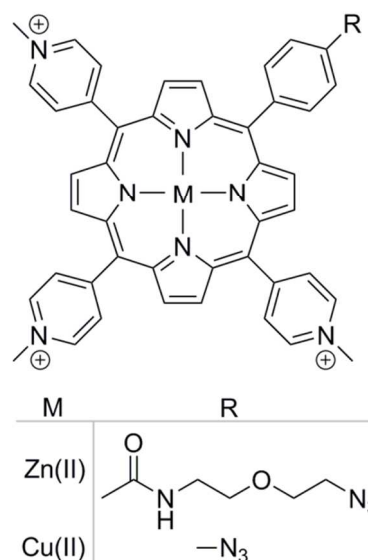
controlled amounts of ROS upon irradiation with visible light. Nanoparticles were doped with cationic chemical groups, to improve sub-cellular localization and delivered to human mesenchymal stem cells (hMSCs). hMSCs do not constitutively produce ROS or have a role in phagocytosis and therefore are a good candidate to study the effects of cumulative ROS. Control over ROS generation was demonstrated by: (1) attenuating the percentage of porphyrins on the nanoparticle surface and (2) modulating the number of light irradiation doses to the internalized nanoparticles. The degree of ROS production was visualized through use of a newly synthesized dye, which is chemically transformed into a fluorescent entity in the presence of ROS. The cytotoxic effects and possible phenotypic changes induced by intracellular ROS generation on hMSCs were investigated using flow cytometry.

2. Results and Discussion

2.1 Synthesis and Characterisation of Porphyrin Functionalized Nanoparticles

Two different porphyrins metal complexes, Zn (II) and Cu (II), were utilised as part of this study, Scheme 1. The ability of Zn (II) porphyrins to generate ROS upon irradiation with visible light has been well characterised,³⁵ whereas Cu (II) complexes do not display phototoxicity.³⁶ The difference in activity is due to the intrinsic electronic properties of the metal-porphyrin complex. The presence of metal ions in the porphyrin macrocycle favours intersystem crossing and allows the excited species to reach a triplet state. For Zn (II) porphyrins, the triplet state lifetime is long enough to allow energy transfer to molecular oxygen, thus generating singlet oxygen, a Type (II) photosensitisation. In contrast, the triplet state lifetime of Cu (II) porphyrins is short and quickly decays back to the ground state, preventing the generation of singlet oxygen by energy transfer.³⁷ Due to the differences in activity, the Cu (II) porphyrin functionalized nanoparticles were utilised as a to the Zn (II) porphyrin functionalized nanoparticles alone.

Porphyrins were covalently linked to nanoparticles *via* a Cu (I)-catalysed alkyne-azide cycloaddition reaction.³⁵ The percentage of nanoparticle functionalization was determined by titrating



Scheme 1. Chemical structure of azide functionalized cationic porphyrin with Zn (II) and Cu (II) metal centres.

alkyne functionalized nanoparticles with porphyrin azides. Nanoparticles saturated with porphyrin were considered to be 100 % functionalized. Nanoparticles functionalized with 5, 10 and 20 % Zn (II) or Cu (II) porphyrins were prepared with nanoparticle diameters centred at 80 nm and positive surface charge to facilitate subcellular localisation (zeta potential > +15 mV) (see supporting information Figure S2 and S3).

2.2 Delivery of Porphyrin Functionalized Nanoparticles

To determine the subcellular localisation of the nanoparticles, analyses were performed on hMSCs treated with Zn (II) porphyrin (5%) functionalized nanoparticles, and stained with LysoTracker[®] blue and MitoTracker[®] green. **Figure 1A** shows a representative merged channel image of Zn (II) porphyrin functionalized nanoparticles delivered to hMSCs. The insets show the individual channels; (Ai) brightfield, (Aii) LysoTracker[®] (blue), (Aiii) MitoTracker[®] (green) and (Aiv) Zn

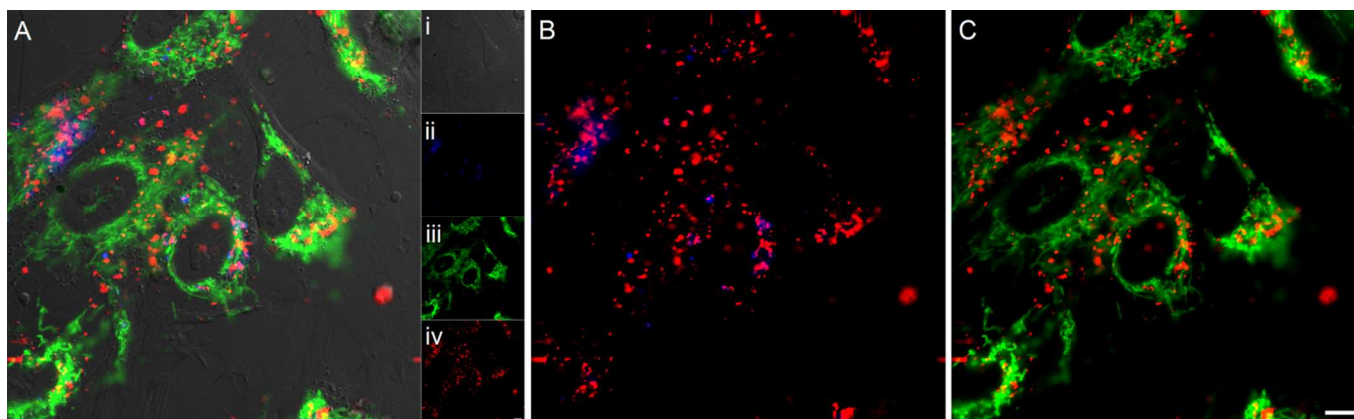
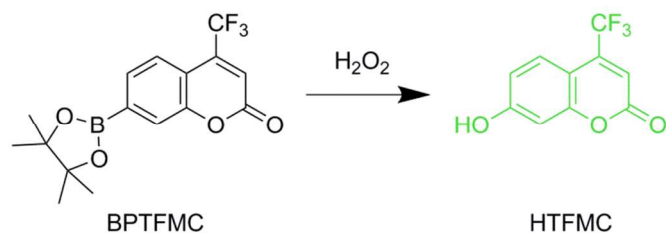


Fig 1. (A) Merged fluorescence image of (Ai) bright-field image of hMSCs treated with (Aii) LysoTracker[®] blue, (Aiii) MitoTracker[®] green and (Aiv) Zn (II) porphyrin conjugated nanoparticles (red) (see supporting information Figure S6 for larger images of Ai-iv). Co-localisation analysis between (B) Zn (II) porphyrin conjugated nanoparticles and LysoTracker[®] blue, and (C) Zn (II) porphyrin conjugated nanoparticles and MitoTracker[®] green. Scale bar = 10 μ m.



Scheme 2. Reaction between non-fluorescent 7-(4,4,5,5-tetramethyl-1,3,2-dioxaborolan-2-yl)-4-(trifluoromethyl)-2H-chromen-2-one (BPTFMC) and ROS producing fluorescent -hydroxy-4-(trifluoromethyl)-2H-chromen-2-one (HTFMC). HTFMC peak excitation and emission wavelengths are 340 nm and 500 nm, respectively.

(II) porphyrin conjugated nanoparticles (*red*). Separation of the fluorescence channels to observe co-localisation of Zn (II) porphyrin functionalized nanoparticles with the mitochondria, Figure 1B, and lysosomes, Figure 1C, facilitates characterisation of the subcellular location.

The lysosomes, as highlighted by LysoTracker[®] blue, appear in punctate vesicles that are co-localised in regions with Zn (II) porphyrin functionalized particles (Pearson's correlation coefficient (PCC) = 0.318 Figure 1B). The nanoparticles are internalized efficiently as highlighted by the strong signal observed in the red fluorescence channel (Figure 1Aiv). The mitochondria, identified by MitoTracker[®] green, are distributed throughout the cytoplasm and are also co-localised with Zn (II) porphyrin conjugated nanoparticles (PCC=0.216 Figure 1C). The images comprising Figure 1 indicate porphyrin functionalized nanoparticles are internalised and associate with lysosomes and mitochondria. Endosomal/ lysosomal escape is thought to occur via disruption of osmotic gradients by surface amine functional groups,³⁸ whereas mitochondrial association is likely to be a result of interaction between the positively charged nanoparticle and the negatively charged mitochondrial membrane.³⁹

2.3 Fluorescence Imaging of ROS Production

A novel dye, 7-(4,4,5,5-tetramethyl-1,3,2-dioxaborolan-2-yl)-4-(trifluoromethyl)-2H-chromen-2-one (BPTFMC), was used to determine the ability of the Zn (II) porphyrin functionalized nanoparticles to generate ROS. BPTFMC is transformed in the presence of hydrogen peroxide (H_2O_2) to the fluorescent entity 7-hydroxy-4-trifluoromethyl-coumarin (HTFMC), Scheme 2 (see supporting information Figures S6-S8). Visualisation of HTFMC fluorescence in subcellular spaces can therefore be utilised as an indirect indicator for cumulative ROS production.

2.4 Controlled ROS Generation in hMSCs

Controlled ROS production in hMSCs was demonstrated through: (1) irradiation of internalised nanoparticles with increasing percentages of Zn (II) porphyrin (5, 10 and 20 %), with a single dose of excitation light and (2) irradiation of internalised nanoparticles, functionalized with 5% Zn (II) porphyrin, with repeated doses of excitation light.

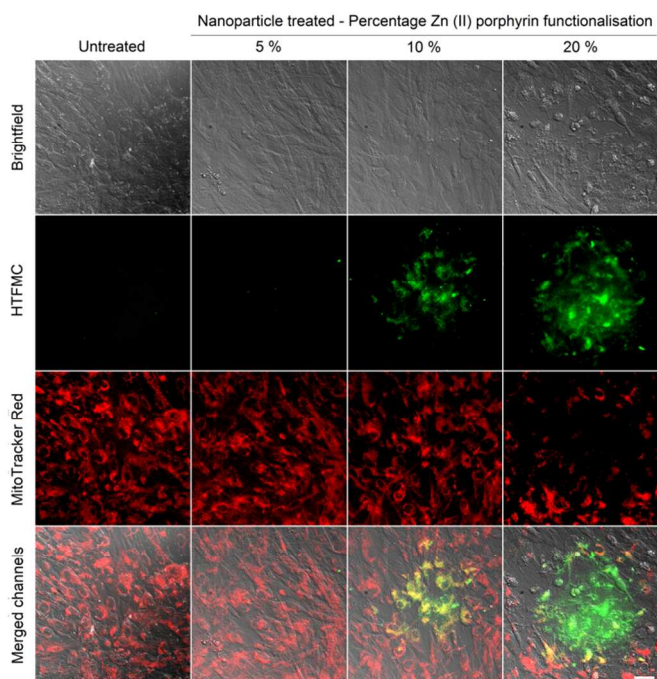


Fig 2. Bright-field and fluorescence images of untreated hMSCs and hMSCs treated with 5, 10 and 20 % Zn (II) functionalized nanoparticles, stained with BPTFMC and MitoTracker[®] Red, irradiated with a single dose of light. BPTFMC, in the presence of H_2O_2 , is converted to fluorescent HTFMC. Scale bar = 50 μm .

The effect of a single dose of excitation light on internalised nanoparticles bearing 5, 10 and 20 % of Zn (II) porphyrin was investigated. hMSCs were treated with nanoparticle suspensions after which they were thoroughly washed to remove non-internalised nanoparticles then stained with BPTFMC and MitoTracker[®] red; to observe ROS production events and location of viable mitochondria in sub-cellular spaces, respectively.

After irradiation with a single dose of light (512 μW , 8mm², 2 seconds), an increase in the fluorescence intensity from HTFMC (*green*) was observed, which correlates with percentage increases in Zn (II) porphyrin conjugated to the nanoparticle, Figure 2. The extent of cytotoxicity caused by the ROS production was demonstrated by the fluorescence response from MitoTracker[®] red, which emits a fluorescence response when bound to viable mitochondrial membranes with active membrane potentials.⁴⁰ Figure 2 highlights the presence of a 'blast zone' within which substantial amounts of ROS has been produced, whilst the number of cells with active mitochondrial membrane potentials has been considerably reduced. The extent of the lethality of high percentages of Zn (II) porphyrin is demonstrated by hMSCs treated with 20 % Zn (II) porphyrin, which show a clear perimeter between viable and non-viable cells. Therefore, the extent of ROS production and consequential cytotoxicity, as indicated by enhanced HTFMC and diminished MitoTracker[®] red fluorescence, respectively, is profoundly influenced by increases in the percentage of porphyrin functionalization.

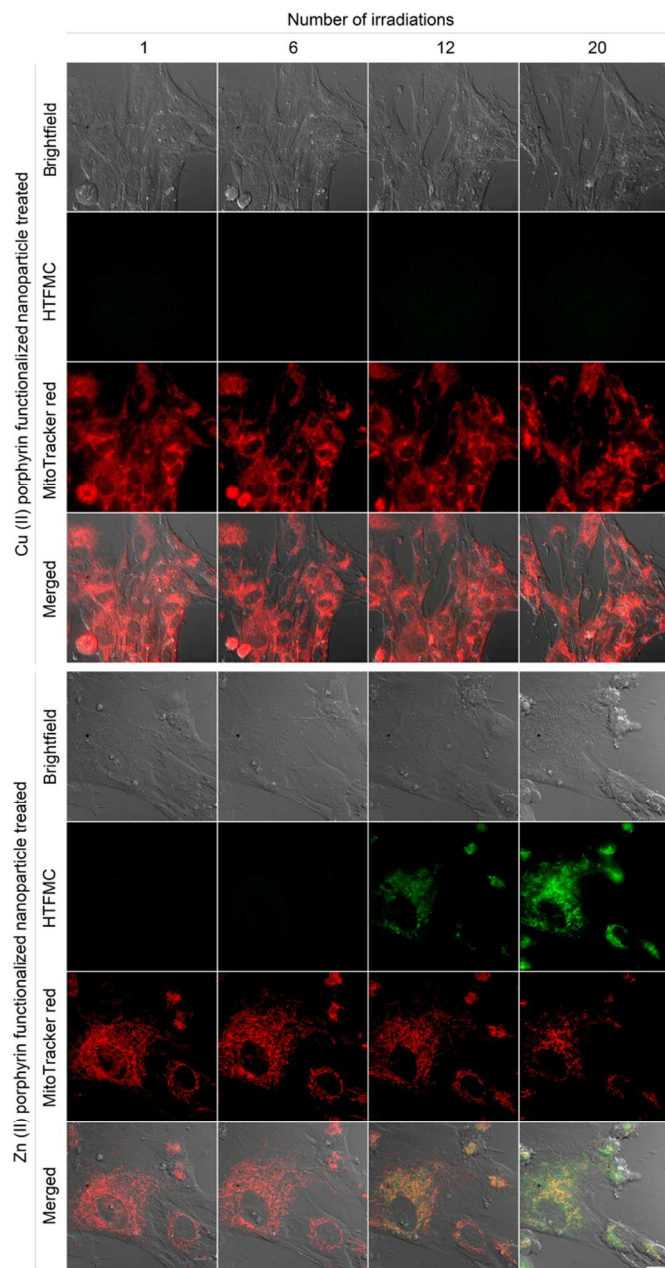


Fig 3. Bright-field and fluorescence images of hMSCs with internalised Cu (II) (control) and Zn (II) functionalized nanoparticles (photosensitiser) and merged fluorescence images of hMSCs stained with BPTFMC and MitoTracker[®] red. Green and red channels are indicative of HTFMC fluorescence and corresponding ROS production and active mitochondrial membrane potentials and cell viability, respectively. Scale bar = 20 μ m.

A single dose of excitation light produced subtle increases in ROS for hMSCs treated with nanoparticles functionalized with 5% Zn (II) porphyrin, Figure 2. To investigate if ROS production can be augmented in a controlled manner, internalised nanoparticles functionalized with 5% Zn (II) porphyrin were subjected to repeat doses of excitation light. hMSCs were irradiated with a dose of excitation light every 5

minutes for 100 minutes. The progress of cellular events was captured at 5, 30, 60 and 100 minutes, corresponding to 1, 6, 12 and 20 irradiations, respectively, Figure 3. hMSCs treated with 5% Cu(II) functionalized porphyrins show no observable differences in cellular morphology, increases in ROS production or cytotoxicity after 20 irradiations, as indicated by brightfield images, absence of HTFMC and similarity of fluorescence emission from MitoTracker[®] red across all time points, respectively. This observation is also true for hMSCs treated with nanoparticles functionalized with 5% Zn (II) porphyrin after a single dose of excitation light.

The first signs of ROS generation appear after 6 irradiations for hMSCs treated with 5% Zn (II) functionalized nanoparticles, Figure 3 (*green*). At these low levels of ROS, there are no apparent changes in cellular toxicity, as there are no noticeable changes in cellular morphology or fluorescence intensity from MitoTracker[®] red. After 12 irradiations, ROS production and its cytotoxic effects are evident, as the fluorescence intensity of HTFMC is pronounced; the signal from the MitoTracker[®] red begins to decrease and the first signs of apoptotic blebbing can also be observed on cell surfaces (Figure 3). For hMSCs dosed with 20 irradiations of excitation light the signal from HTFMC was intensified further, suggesting sub-cellular spaces were being enriched with ROS. In addition, the MitoTracker[®] red emission was greatly diminished, implying that the number of active mitochondrial membrane potentials was reduced; and there also are more signs of a decline in cellular viability, as bright field images showed signs of increases in apoptotic blebbing, Figure 3.

2.5 Effects of Controlled Intracellular ROS Generation on hMSCs Characterisation

Flow cytometry was employed to quantify the viability and any phenotypic variation in hMSC populations treated with Zn (II) porphyrin functionalized nanoparticles and after illumination with repeated doses of light (produced using a custom designed irradiator that replicated the power and wavelength of excitation light used during fluorescence microscopy, see supporting information). Cell viability, apoptosis (controlled cell death), necrosis (uncontrolled cell death), and cellular differentiation were investigated through the use of fluorescent probes. Apoptosis was investigated using Annexin V Alexa Flour[®] 488, which binds to cell surface markers that are translocated during apoptosis.⁴¹ Whereas, necrosis was determined using the DNA intercalator propidium iodide, which stains deteriorating cells with permeable membranes.⁴² The effect of intracellular ROS on hMSCs phenotype was studied using fluorescent antibodies for specific cell surface markers.^{43, 44}

Figure 4 shows there are no significant differences in the percentage of apoptotic and necrotic cells for (1) untreated and (2) Cu (II) porphyrin functionalized nanoparticle treated hMSC populations, after irradiation with 5 to 20 doses of excitation light (approximately 20% of the population express markers for apoptotic events that can be attributed to cell death during storage and thawing). However, hMSCs treated with Zn (II) porphyrin functionalized particles demonstrate statistically significant increases in the population of apoptotic cells when compared to (1) untreated and Cu(II) functionalized nanoparticle treated hMSCs ($p < 0.05$) and (2) after repeated irradiation with excitation light ($p < 0.001$). Dosing hMSCs with

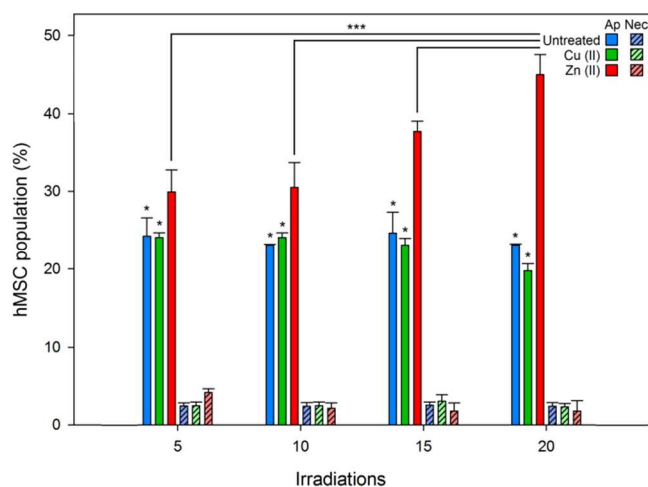


Fig 4. Comparison of untreated (blue) and 5% Cu (II) (green) or 5% Zn (II) (red) functionalized nanoparticle treated hMSC populations undergoing apoptosis (Ap, solid) and necrosis (Nec, diagonal lines) after 5, 10, 15 and 20 irradiations of excitation light. Percentage of apoptosis and necrosis was determined using flow cytometry by staining apoptotic hMSCs with Annexin V 488 and propidium iodide, respectively. Error bars represent standard deviation from the mean (n=6). One Way ANOVA *** = $p < 0.001$; One way ANOVA * = $p < 0.05$. P values less than 0.05 were considered statistically different.

5, 10, 15 and 20 irradiations of excitation light increases the percentage of apoptotic cells to 29, 30, 37 and 44 %, respectively (n=6). We postulate that the percentage of apoptotic cells does not increase at low irradiation levels due to the natural antioxidant levels present in the cell (5 to 10 irradiations).⁴⁵ However, once this antioxidant reservoir is exhausted it is noticeable the percentage of apoptotic cells increases linearly with light irradiations (10 to 20 irradiations).

Populations of untreated hMSCs and Cu (II) or Zn (II) porphyrin functionalized nanoparticles treated hMSCs contained low levels of propidium iodide positive cells; less than 5% of total population, Figure 4. There were no significant differences between the hMSC populations after repeated doses of excitation light, from 5 to 20 irradiations. These findings suggest repeated irradiation of internalised Zn (II) porphyrin functionalized nanoparticles generate doses of ROS that signal hMSCs to undergo controlled apoptotic cell death rather than uncontrolled necrotic cell death. These observations also mirror findings observed in Figure 3, which show signs of apoptotic blebbing, rather than necrotic cell lysis.

Phenotypic characterisation of hMSCs was explored, by labelling cell surface markers with fluorochoime-conjugated antibodies, after 20 irradiations of excitation light and two cellular passages. Phenotypic characterisation of hMSCs showed untreated hMSCs and, Cu (II) or Zn (II) porphyrin functionalized nanoparticle treated hMSCs presented virtually identical phenotypic profiles (see supporting information Figure S10 & S11). These results suggest that irradiation of Zn (II) porphyrin functionalized nanoparticles and subsequent ROS generation does not change the phenotype or induce senescence patterns in hMSCs.

3. Conclusion

In summary, we have demonstrated that upon illumination nanoparticles functionalized with Zn (II) porphyrin trigger intracellular ROS production. The intracellular effects of enhanced ROS production were evidenced through visualisation using BPTFMC, which is transformed into fluorescent HTFMC in the presence of H_2O_2 , and observation of diminishing mitochondrial membrane potentials, using MitoTracker[®] red. Increases in: (1) the percentage of Zn (II) porphyrin conjugated to nanoparticles, from 5 to 20 %, and (2) the number of irradiations of excitation light, enhanced ROS production and subsequent cytotoxicity. Controlled irradiation of Zn (II) porphyrin functionalized nanoparticles was found to signal apoptosis in hMSCs, but did not induce necrosis or phenotypic changes in hMSC subcultures. The Zn (II) porphyrin functionalized nanoparticles described in this article exhibit two key advances: (1) the level of ROS can be modulated to a desired oxidative stress level, through control of either photosensitiser concentration or light dose, and (2) they are applicable to virtually all biological systems, as they operate independent of specific cell enzymes to generate ROS. For this reason, we anticipate porphyrin functionalized nanoparticles will prove to be a valuable tool to generate controlled amounts of intracellular ROS to advance the study of cellular processes and disease progression.

Acknowledgements

The authors would like to thank the EPSRC for funding this work through grants EP/H000151/1 (RWB & FG) , EP/H002421/1 (AB), and EP/G069972/1 (JWA and ASL) The authors would also like to acknowledge Damascus University, Syria for funding (AAZ).

Notes and references

^a Laboratory of Biophysics and Surface Analysis, School of Pharmacy, Boots Science Building, University of Nottingham, Nottingham, NG7 2RD, UK.

^b School of Pharmacy, Centre for Biomolecular Sciences, University of Nottingham, Nottingham, NG7 2RD, UK.

^c School of Pharmacy & Biomolecular Sciences, Liverpool John Moores University, James Parsons Building, Byrom Street, Liverpool, L3 3AF, UK.

^d Department of Research & Development of Next Generation Medicine, Faculty of Medical Sciences, Kyushu University, Biomedical Research Station 211, 3-1-1 Maidashi, Higashi-Ku, Fukuoka, 812-8582, Japan.

^e University of Hull, Department of Chemistry, Hull, HU6 7RX, UK.

^f Durham University, Department of Chemistry, Durham, DH1 3LE, UK.

ASL synthesized and characterized Cu (II) and Zn (II) porphyrin conjugated nanoparticles; conducted cell experiments, fluorescence microscopy, flow cytometry and data analysis; designed and fabricated custom irradiator. VMC wrote the article, prepared figures and supporting information performed data analysis, and conducted image processing. AAZ synthesized and

characterized BPTFMC and HTFMC. FG synthesized Cu (II) and Zn (II) complexed porphyrins. DREJ provided guidance on storage, maintenance and characterization of hMSCs. All authors contributed to scientific planning, direction and discussion.

† Electronic Supplementary Information (ESI) available: Materials and experimental methods for the synthesis of (1) positively charged alkyne functionalized nanoparticles (2) Zn (II) and Cu (II) centred porphyrin (3); conjugating porphyrins to alkyne-functionalized nanoparticles *via* click chemistry (4) nanoparticle characterisation (size charge and fluorescence), (5) synthesis of BPTFMC (6) hMSC collection, storage and preparation (7) delivery of porphyrin functionalized nanoparticles (8) staining mitochondria, cumulative ROS production and determination of nanoparticles subcellular localisation (9) fluorescence microscopy and controlled irradiation of hMSCs (10) flow cytometry and controlled irradiation using a custom built irradiator. In addition, results highlighting: (1) nanoparticles emission spectra, size and charge, (2) BPTFMC fluorescence response and (3) hMSCs following light irradiation using flow cytometry. See DOI:10.1039/b000000x/

References

1. K. Apel and H. Hirt, *Annual Review of Plant Biology*, 2004, **55**, 373-399.
2. J. F. Turrens, *Journal of Physiology-London*, 2003, **552**, 335-344.
3. P. Karihtala and Y. Soini, *Apmis*, 2007, **115**, 81-103.
4. H. U. Simon, A. Haj-Yehia and F. Levi-Schaffer, *Apoptosis*, 2000, **5**, 415-418.
5. M. A. Torres, J. D. G. Jones and J. L. Dangl, *Plant Physiology*, 2006, **141**, 373-378.
6. Y. B. Liu, G. Fiskum and D. Schubert, *Journal of Neurochemistry*, 2002, **80**, 780-787.
7. H. Kamiya, *Nucleic Acids Research*, 2003, **31**, 517-531.
8. B. S. Berlett and E. R. Stadtman, *Journal of Biological Chemistry*, 1997, **272**, 20313-20316.
9. R. J. Aitken, J. S. Clarkson and S. Fishel, *Biology of Reproduction*, 1989, **41**, 183-197.
10. N. Festjens, T. Vanden Berghe and P. Vandenabeele, *Biochimica Et Biophysica Acta-Bioenergetics*, 2006, **1757**, 1371-1387.
11. G. Waris and H. Ahsan, *Journal of carcinogenesis*, 2006, **5**, 14-14.
12. B. Uttara, A. V. Singh, P. Zamboni and R. T. Mahajan, *Current Neuropharmacology*, 2009, **7**, 65-74.
13. H. J. Forman, *Free Radical Biology and Medicine*, 2007, **42**, 926-932.
14. V. de Oliveira-Marques, L. Cyrne, H. S. Marinho and F. Antunes, *Journal of Immunology*, 2007, **178**, 3893-3902.
15. E. W. Miller, B. C. Dickinson and C. J. Chang, *Proceedings of the National Academy of Sciences of the United States of America*, 2010, **107**, 15681-15686.
16. B. K. Huang and H. D. Sikes, *Redox Biology*, 2014, **2**, 955-962.
17. A. P. Wojtovich and T. H. Foster, *Redox Biology*, 2014, **2**, 368-376.
18. H. Pelicano, D. Carney and P. Huang, *Drug Resistance Updates*, 2004, **7**, 97-110.
19. A. T. Dharmaraja and H. Chakrapani, *Org. Lett.*, 2014, **16**, 398-401.
20. A. Grzelak, B. Rychlik and G. Bartosz, *Free Radical Biol. Med.*, 2001, **30**, 1418-1425.
21. K. Berg, A. Weyergang, L. Prasmickaite, A. Bonsted, A. Høgset, M.-T. Strand, E. Wagner and P. Selbo, in *Photodynamic Therapy*, ed. C. J. Gomer, Humana Press, 2010, vol. 635, ch. 10, pp. 133-145.
22. J. W. Aylott, *Analyst*, 2003, **128**, 309-312.
23. A. S. Desai, V. M. Chauhan, A. P. R. Johnston, T. Esler and J. W. Aylott, *Frontiers in Physiology*, 2013, **4**, 401-401.
24. R. V. Benjaminsen, H. Sun, J. R. Henriksen, N. M. Christensen, K. Almdal and T. L. Andresen, *ACS Nano*, 2011, **5**, 5864-5873.
25. F. Giuntini, V. M. Chauhan, J. W. Aylott, G. A. Rosser, A. Athanasiadis, A. Beeby, A. J. MacRobert, R. A. Brown and R. W. Boyle, *Photochemical & Photobiological Sciences*, 2014, **13**, 1039-1051.
26. Y. E. K. Lee, R. Smith and R. Kopelman, *Annual Review of Analytical Chemistry*, 2009, **2**, 57-76.
27. V. M. Chauhan, G. R. Burnett and J. W. Aylott, *Analyst*, 2011, **136**, 1799-1801.
28. P. G. Coupland, S. J. Briddon and J. W. Aylott, *Integrative Biology*, 2009, **1**, 318-323.
29. H. A. Clark, M. Hoyer, S. Parus, M. A. Philbert and M. Kopelman, *Mikrochimica Acta*, 1999, **131**, 121-128.
30. T. Doussineau, A. Schulz, A. Lapresta-Fernandez, A. Moro, S. Koersten, S. Trupp and G. J. Mohr, *Chemistry-a European Journal*, 2010, **16**, 10290-10299.
31. V. M. Chauhan, G. Orsi, A. Brown, D. I. Pritchard and J. W. Aylott, *ACS nano*, 2013, **7**, 5577-5587.
32. H. K. Yoon, X. Lou, Y.-C. Chen, Y.-E. K. Lee, E. Yoon and R. Kopelman, *Chemistry of Materials*, 2014, **26**, 1592-1600.
33. M. Kuruppuarachchi, H. Savoie, A. Lowry, C. Alonso and R. W. Boyle, *Mol. Pharm.*, 2011, **8**, 920-931.
34. C. A. Robertson, D. H. Evans and H. Abrahamse, *J. Photochem. Photobiol. B: Biol.*, 2009, **96**, 1-8.
35. F. Giuntini, F. Dumoulin, R. Daly, V. Ahsen, E. M. Scanlan, A. S. P. Lavado, J. W. Aylott, G. A. Rosser, A. Beeby and R. W. Boyle, *Nanoscale*, 2012, **4**, 2034-2045.
36. G. Szintay and A. Horvath, *Inorganica Chimica Acta*, 2001, **324**, 278-285.
37. M. Ochsner, *J. Photochem. Photobiol. B: Biol.*, 1997, **39**, 1-18.
38. J. E. Fuller, G. T. Zugates, L. S. Ferreira, H. S. Ow, N. N. Nguyen, U. B. Wiesner and R. S. Langer, *Biomaterials*, 2008, **29**, 1526-1532.
39. C. Pavani, A. F. Uchoa, C. S. Oliveira, Y. Iamamoto and M. S. Baptista, *Photochemical & Photobiological Sciences*, 2009, **8**, 233-240.
40. W. Pendergrass, N. Wolf and M. Poot, *Cytometry Part A*, 2004, **61A**, 162-169.
41. I. Vermes, C. Haanen, H. Steffensnakken and C. Reutelingsperger, *Journal of Immunological Methods*, 1995, **184**, 39-51.
42. H. Sawai and N. Domae, *Biochemical and Biophysical Research Communications*, 2011, **411**, 569-573.
43. R. Gaebel, D. Furlani, H. Sorg, B. Polchow, J. Frank, K. Bieback, W. Wang, C. Klopsch, L.-L. Ong, W. Li, N. Ma and G. Steinhoff, *Plos One*, 2011, **6**.
44. E. A. Jones, S. E. Kinsey, A. English, R. A. Jones, L. Straszynski, D. M. Meredith, A. F. Markham, A. Jack, P. Emery and D. McGonagle, *Arthritis and Rheumatism*, 2002, **46**, 3349-3360.
45. H. Yagi, J. Tan and R. S. Tuan, *Journal of Cellular Biochemistry*, 2013, **114**, 1163-1173.